Aerosol Transport and Source Attribution Using Sunphotometers, Models and *In-Situ* Chemical Composition Measurements

Daniela Viviana Vladutescu, Bomidi Lakshmi Madhavan, Barry M. Gross, Qi Zhang, and Shan Zhou

***Abstract*—Understanding of chemical, physical, and radiative processes—emissions, transport, deposition, and modification of aerosol optical properties due to ageing—is of major importance to global and regional climate simulations and projections as well as health impairment. This paper presents aerosol optical properties retrieved with the Multifilter Rotating Shadowband Radiometers (MFRSRs) and the source attribution based on back trajectories and *in situ* aerosol chemical composition analysis obtained during the Aerosol Life Cycle Intensive Observational Period at Brookhaven National Laboratory on Long Island, NY, during July and August 2011. The aerosol optical properties retrieved with the MFRSR exhibit excellent agreement with those obtained with a colocated Cimel sunphotometer. Apportioning aerosol optical depths by size modes reveals several episodes of high loading of fine aerosol (diameter less than 2.5 μm). Analysis of optical and physical properties of aerosols as well as their chemical composition obtained by an *in situ* high-resolution time-of-flight aerosol mass spectrometer together with back trajectories indicates that the principal source of high concentrations of fine aerosols observed during July 18–24 was forest fires in western Canada, consistent with reports by the Canadian Forest Service and satellite observations by the Moderate Resolution Imaging Spectroradiometer (MODIS).**

***Index Terms*—Aerosol mass spectrometry, aerosol optical depth, aerosol size modes, Cimel, Multifilter Rotating Shadowband Radiometer (MFRSR), sunphotometer, transport.**

I. Introduction

ATMOSPHERIC aerosols are suspensions of small solid and/or liquid particles in air. The scattering and absorption by aerosols contribute to the extinction of the solar radiation passing through the atmosphere. The amount of scattered or absorbed radiant intensity is linearly proportional to the intensity of the radiation at that point along the ray path, the local concentration of gases or particles responsible for absorption and scattering, and the absorption and scattering coefficients of the substances. The aerosol particles present in the atmosphere vary in shape and chemical composition based on the sources. Variation in these properties leads to variation in the refractive index of aerosol particles, light scattering, and absorption coefficients, all of which are wavelength dependent. Consequently, the variability of these properties affords the possibility of remote sensing of aerosol properties in addition to optical depth, which is manifested only by reduction in the intensity of the direct beam. Scattering enhances the diffuse radiation. Therefore, measurements of diffuse and direct radiation are essential to the remote sensing of the physical and optical properties of aerosols.

Solar radiometric measurements are very useful for the retrieval of both extensive and intensive properties of atmospheric aerosols; extensive properties scale with the amount of the aerosol, whereas intensive properties are independent of the amount and generally describe relationships among various aerosol properties [1]. Understanding of properties of aerosols and the modification of these properties as aerosols are transported is an important factor in quantifying their effect on climate and climate change. More specifically, these properties are central for modeling radiative forcings due to aerosols and subsequent quantitative estimates of aerosol influences on the Earth radiation budget [2], [3]. In addition, fine-mode aerosols (often denoted as $PM_{2.5}$ representing particles having diameter < 2.5 μm), besides being a rough proxy for anthropogenic aerosols, can result in respiratory and pulmonary distress in humans [4]. For these reasons, it is very useful to identify and characterize episodes with high concentrations of fine particulate matter [5], [6]. Two widely used field-tested instruments that measure column aerosol optical properties are 1) the Multifilter Rotating Shadowband Radiometer (MFRSR) [7]–[11] and 2) the Cimel sunphotometer [12]–[14]. The MFRSR, which measures the total and diffuse components of the downwelling solar irradiance at six different wavelengths, is extensively used by the Department of Energy (DOE) Atmospheric Radiation Measurement (ARM) Program [15], NASA Solar Irradiance Research Network (SIRN) [15], NOAA Surface Radiation (SURFRAD) Network [17], and U.S. Department of Agriculture (USDA) UV monitoring network [18], [19]. Worldwide, the MFRSR is also used by the Australian Bureau of Meteorology Solar and Terrestrial Network [20], [21] and the Baseline Surface Radiation Network (BSRN), a project of World Climate Research Programme (WCRP) and the Global Energy and

Manuscript received March 28, 2012; revised October 9, 2012; accepted October 29, 2012. Date of publication January 29, 2013; date of current version June 20, 2013. The work of Q. Zhang and S. Zhou was supported by the U.S. Department of Energy Atmospheric Systems Research (ASR) Program under Grant DE-FG02-11ER65293.

D. V. Vladutescu is with the Electrical and Telecommunications Engineering Technology Department, New York City College of Technology/City University of New York, Brooklyn, NY 11201 USA (e-mail: vvladutescu@citytech.cuny.edu; vivianavladutescu@yahoo.com).

B. L. Madhavan is with the Department of Chemical Engineering, Indian Institute of Technology Bombay, Mumbai 400 076, India.

B. M. Gross is with the Department of Electrical Engineering, City College of New York, New York, NY 10031 USA.

Q. Zhang is with the Department of Environmental Toxicology, University of California, Davis, CA 95616 USA.

S. Zhou is with the Atmosphere Science Graduate Group, University of California, Davis, CA 95616 USA.

Digital Object Identifier 10.1109/TGRS.2012.2227489

Water Experiment (GEWEX) [22]. The Cimel sunphotometers are widely deployed by the NASA Aerosol Robotic Network (AERONET) [23] to determine atmospheric extinction and microphysical properties that are critical in evaluating satellite retrievals of these properties [5].

For air quality applications (i.e., inhalation), direct surface sampling techniques have the advantage of providing detailed information on the size distributions and size-dependent composition. On the other hand, optical remote sensing methods obtain column-integrated aerosol properties pertinent to the radiative effects of aerosols on local environments. In this paper, we make use of sunphotometers to provide reliable measurements of multispectral optical depth and apportioning of aerosols into fine and coarse modes pertinent to source attribution.

The focus of this paper is on the measurement of both AOD and fine/coarse-mode apportionment during an intensive observation period (IOP) examining aerosol optical, chemical, and microphysical properties and radiative influences conducted at Brookhaven National Laboratory in semirural Eastern Long Island during July and August 2011. In particular, we are interested in identifying periods of enhanced AOD, which may be linked to meteorological conditions responsible for transport of exogenous aerosol to the Long Island site. Interpretation of the source of aerosol present in these episodes is greatly enhanced by simultaneous measurement of the size-dependent chemical composition of the particulate matter. Here, this is accomplished using a high-resolution time-of-flight aerosol mass spectrometer (HR-ToF-AMS), which is capable of *in situ* determination of the size-resolved chemical composition of submicrometer nonrefractory (NR) aerosols with a time resolution of a few minutes or better [22]–[24]. Compared with filter measurements, which usually offer data with time resolution of one day or, at best, a few hours, the high time resolution of mass spectrometric data is particularly powerful in revealing details about variations aerosol composition that are key to understanding the physico-chemical processes of atmospheric aerosols [26]–[28].

This paper is organized as follows: The main characteristics of the instrumentation used are presented in Section II. Section III discusses the methods for retrieving the aerosol optical properties. Section IV discusses the results, and the conclusions are presented in Section V.

II. Instruments

A. Remote Sensing Instruments for Aerosol Properties

Sun photometry has been used for measuring atmospheric properties since 1666, when Newton conducted the first investigations on the spectrum of solar radiation [29], [30]. In modern remote sensing, the instruments used for detecting solar radiation are sunphotometers such as those as mentioned in the introduction section. The MFRSR [see Fig. 1(a)] collects total and diffuse solar irradiance in seven bands: six narrow bands nominally centered at 415, 496, 613, 672, 868, and 938 nm and a broadband channel (300–2700 nm). For aerosol applications, only the first five channels are used. Although these channels are mainly sensitive to aerosols, there are small contributions due to ozone (O_3) and nitrogen dioxide (NO_2) that must be accounted for. In particular, ozone has contributions at 496, 613, and 672 nm, and NO_2 has contributions at 413, 496, and 613 nm. Details of the processing of the MFRSR data are given in the methods section.

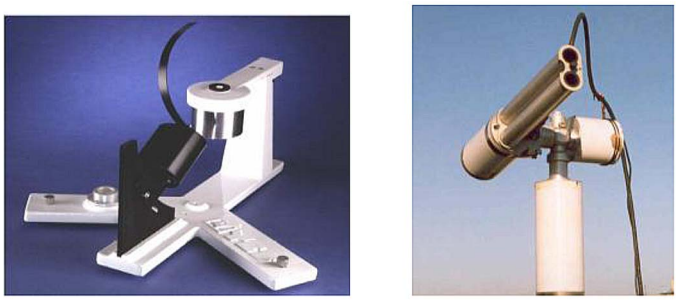

(a) (b)

Fig. 1. Sunphotometers used in the characterization of atmospheric aerosols. (a) MFRSR. (b) Cimel sunphotometer.

MFRSR: The main components of the MFRSR are the sensor head and the shadowband. The shadowband [see Fig. 1(a)] is a strip of metal formed into a circular arc and mounted along a celestial meridian, with the entrance aperture (diffuser) of the instrument located behind the center of the arc. The shadowband blocks a strip of sky with a 3.3° umbral angle, enough to block the sun. The accuracy of the shadowband position, i.e., 0.4°, is achieved with the help of a microprocessor-controlled stepper motor. This microprocessor controls the instrument overall. At each measurement interval, the instrument computes the solar position using an approximation of the solar ephemeris. The first measurement is made with the band rotated to its nadir position to obtain the global or total irradiance. The band is then rotated to make three more measurements. The second measurement (the diffuse-horizontal irradiance) is made with the sun completely blocked; the other two are made with the band rotated 9° to either side of the sun. These side measurements allow correcting for the excess sky that is blocked by the shadowband during the sun-blocked measurement [16]. The data acquisition software subtracts the corrected diffuse component of the downwelling irradiance from the global irradiance to obtain the downwelling irradiance of the direct (solar) beam. It then divides this direct component of the downwelling horizontal irradiance by the cosine of the solar zenith angle (available from the ephemeris calculation) to compute the direct normal solar irradiance (DNSI), i.e., the irradiance incident on a plane normal to the vector to the sun. The sequence takes 20 s, and therefore, sampling can be as fast as three times per minute.

Total optical depth (TOD), i.e., τ_{T}, is obtained from the measurements by the Beer–Lambert law. Thus

$$I = I_0 e^{(-\tau_{\mathrm{T}} m)} \tag{1}$$

where I_0 is the irradiance of the direct solar beam for a given filter channel that would be measured by the instrument in the absence of an atmosphere (denoted top of the atmosphere solar irradiance), I is the actual measured solar irradiance in the same channel, m is the airmass (path length of the direct beam through the atmosphere relative to vertical, evaluated as secant of the solar zenith angle), and τ_{T} is the total vertical

optical depth at that wavelength, which includes scattering and absorption by gases and aerosols. From (1)

$$\tau_{\mathrm{T}} = -\ln(I/I_0)/m \tag{2}$$

from which it is seen that determination of τ_{T} requires knowledge of the top of the atmosphere intensity in addition to the measured intensity.

For a given wavelength channel in a specific sunphotometer, the voltage corresponding to the top of the atmosphere solar irradiance can be determined with calibrated standard lamps [34], [35] or, alternatively, can be directly obtained from the dependence of τ_{T} on airmass (Langley method). Thus, if the voltage output of the detector is proportional to the intensity of radiation on the detector, i.e.,

$$\ln V = \ln V_0 - m\tau_{\mathrm{T}} \tag{3}$$

a plot of $\ln V$ versus m for any channel will have a slope τ_{T} and intercept $\ln V_0$, corresponding to that channel, provided that the optical depth is constant over the period of the measurement and that the direct beam is not obscured by clouds.

Cimel Sunphotometer: The Cimel sunphotometer [34], [35] used for comparison with the MFRSR in this study i [see Fig. 1(b)] was collocated with and performed simultaneous measurements with the MFRSR. The instrument is part of the NASA AERONET (AErosol RObotic NETwork) [36]. This microprocessor-controlled stepper-motor-positioned robot has a two-component optical head containing a sun collimator without lens and a sky collimator with lenses and filter wheel. Sun tracking is controlled with a four-quadrant detector. This instrument measures, based on the attenuation of direct solar radiation, column-integrated extinction, similar to the MFRSR. The direct normal solar irradiance at 340, 380, 440, 500, 670, 870, 936, and 1020 nm measured every 15 min allows for AOD retrievals at these wavelengths. The Cimel instrument is regularly calibrated, yielding an independent measure of I_0 that allows determination of direct beam extinction measurements by (2).

For both instruments, the attenuation of the direct beam includes not only the aerosol contributions but also Rayleigh scattering [31] and molecular absorption by O_3 and NO_2. Therefore, the TOD is expressed as

$$\tau_{\mathrm{T}} = \tau_{\mathrm{aer}} + \tau_{\mathrm{Ray}} + \tau_{\mathrm{O_3}} + \tau_{\mathrm{NO_2}}. \tag{4}$$

From (4), it follows that AOD (τ_{aer}) is obtained by difference.

Sky radiance is measured once an hour at wavelengths corresponding to low gaseous absorption, i.e., at 440, 670, 870, and 1020 nm.

Attribution of AOD into the fine- and coarse-mode AOD components is achieved by a semiempirical approach from the wavelength dependence of the extinction [12]–[14]. The aerosol properties so retrieved (AOD, fine- and coarse-mode AOD) were obtained from AERONET, Data-*Access* and *Dissemination Tools*, http://aeronet.gsfc.nasa.gov/new_web/data.html.

B. In situ Aerosol Composition Measurements

In this paper, an HR-ToF-AMS was used to measure the loadings and size-resolved composition of ambient NR particles with a time resolution of 5 min. The HR-ToF-AMS uses an aerodynamic lens to sample submicrometer particles into vacuum, where they are aerodynamically sized, thermally vaporized on a heated surface ($\sim$600 °C), and chemically analyzed via electron impact ionization ToF mass spectrometry [35]. As aerosol species must be vaporized to be detected, the AMS does not measure refractory materials that have very low vapor pressure at the vaporizer temperature, importantly, mineral dust, elemental carbon, and sea salt. However, NR materials (i.e., sulfate, nitrate, ammonium, organics, and chloride), even if internally mixed with refractory substances, can be determined by the AMS. The HR-ToF-AMS can be operated under two ion optical modes referred to as "V" and "W" according to the ion flight paths. During this study, the V and W modes were alternated every 2.5 min. The V-mode operation determines aerosol speciation at excellent sensitivity (e.g., detection limits of < 20 ng $\cdot$ m^{-3} for all NR-PM species at 5-min integration time. The W-mode offers a higher mass resolution of $\sim$5000–6000 (versus $\sim$2500 of the V-mode), under which elemental composition of most small ions (< 100 amu) can be unambiguously determined, and elemental ratios (O/C, N/C, etc.) of the sampled organic aerosol (OA) material can be inferred [37], [38]. Information about the elemental compositions of OA provides valuable insight into its sources and transformations.

III. Methods

A. Retrieval of Aerosol Optical Properties

The AOD and the apportionment of aerosol optical depth into fine and coarse modes from the measurements are determined by an automated method described in [7] and [39]. This approach first makes use of the combined diffuse and direct irradiance measurements to perform a calibration of this channel; this calibration, which is restricted to situations of cloud-free sky, is transferred to other situations, thereby permits determination of the AOD at 868 nm. Once AOD_{868} is obtained, we make use of the principle that the aerosol intensive parameters such as the spectral extinction ratios are more stable over the course of a day than the extensive AOD. This allows us to perform a regression where the uncalibrated optical depth of a given channel (i) is regressed against the calibrated optical depth of the 868-nm channel. Here, the fixed regression parameters are the calibration constant of the ith channel and the spectral extinction ratio q_i defined as $Q_{\mathrm{ext}}(q_i)/Q_{\mathrm{ext}}(868)$ [7, eq. (12)]. Once the spectral extinctions are obtained, we can use them to extract details of the particle size distribution. The underlying aerosol bimodal model assumes that the complex refractive index is a given constant for both modes, and the coarse-mode effective width, radius and fine-mode width are also fixed. This leaves two variable parameters (the fine-mode radius and the ratio of the fine/coarse-mode volumes) to be determined. By using the spectral extinctions on the 415- and 670-nm channels, a robust retrieval of the remaining size parameters is made [7, Sec. 5]. Knowing the particle size distribution and complex refractive index fixes the aerosol phase function and determines the ratio of fine-mode to coarse-mode AOD.

In performing this analysis, one might be concerned with cloud contamination. According to [39], in processing the

direct irradiance channel, existing cloud clearing approaches are made to the data. In addition, cases where the direct channel is considered cloud-free can still have clouds affecting the diffuse irradiance. However, as mentioned before, the diffuse component is only used in the retrieval of the 868-nm channel. Therefore, the only issue to consider is possible contamination of the 868 AOD that may propagate into the other channels, and it is therefore useful to review the approach to extract the AOD at 868 nm. In the procedure, as outlined in detail in [40], the $\tilde{\tau}_{868}$ (uncalibrated AOD $\tilde{\tau}_{868} = -m * \ln(I)$) is compared with τ_{diff} ("diffuse" AOD). The τ_{diff} is defined to be the AOD of the aerosol model whose direct/diffuse irradiance ratio when calculated using a radiative transfer model agrees with the measured direct/diffuse irradiance ratio. Once we have both $\tilde{\tau}_{868}$ and τ_{diff}, we can use these quantities to find the τ_{868} calibrated AOD and the calibration constant. To do this, the method makes use of the observation that $\tilde{\tau}_{868}$ and τ_{diff} seem to differ by an approximately constant value, which is termed the opacity deficit in [40] (see Fig. 1). In this case, by forming the difference between $\tilde{\tau}_{868}$ and τ_{diff}, (y-axis) and regress this against the standard m (x-axis), we obtain both the calibration constant and the LSQ estimate of the AOD deficit. The final calibrated AOD is then τ_{diff}, added to the deficit AOD (difference).

In analyzing the procedure, we note that cloud contamination will affect the diffuse channel in a way that can cause τ_{diff} to change value while $\tilde{\tau}_{868}$ does not. Therefore, when plotting the residual between $\tilde{\tau}_{868}$ and τ_{diff}, sudden abrupt changes will be seen and were removed, whereas slow (background) effects will simply modify the magnitude of the difference. Because the difference is calculated by regression, these changes do not significantly affect the final AOD.

Contributions to direct beam extinction due to absorption by O_3, NO_2, and Rayleigh scattering must be also taken into account; uncertainties in column burdens of O_3, NO_2, and atmospheric pressure (influencing the calculated Rayleigh scattering extinction [41]) can thus contribute to uncertainty in the determination of AOD from TOD and, in turn, to the determination of fine/course ratio. During the retrieval, small contributions to the extinction of the direct beam due to O_3 and NO_2 were calculated using satellite measurement of total column concentrations. Although it is conceivable that ozone retrieval can be simultaneously with aerosol retrievals [7], [42] indicated that the accuracy on such a retrieval is no better than daily and monthly total ozone column data sets ozone from TOMS (Total Ozone Mapping Spectrometer) observations (http://toms.gsfc.nasa.gov/ftpdata_v8.html), which is what is used. For a typical uncertainty in O_3 column burden of 7×10^{17} molecules cm^{-2}, the uncertainty due to O_3 optical depth is 0.005. NO_2 column burden was obtained from the SCIAMACHY tropospheric product (http://www.iup.uni-bremen.de/doas/scia_no2_data_tropos.htm). If no overpass data are available, monthly mean climatology values are used [7]. This data set was used to produce a NO_2 climatology file for the measurement location, which is considered appropriate for the BNL site because of the absence of proximate major sources of NO_2. A typical column burden of NO_2 of 2×10^{16} molecules cm^{-2} in results in an optical depth in the 415-, 500-, and 615-nm MFRSR channels of 0.011, 0.004, and 0.0007, respectively, on the margins of the OD measurement accuracy of ± 0.01 [7]; it is practically zero at 670 and 870 nm. For calculation of Rayleigh optical depth, a difference of 10 hPa between the actual pressure and the value used in the calculation leads to a difference in optical depth of only 0.004 at the most sensitive wavelength of 415 nm [43]. (Measurements at 415 and 610 nm were not used for comparisons because of the lack of sensors at these wavelengths in the Cimel sunphotometer.)

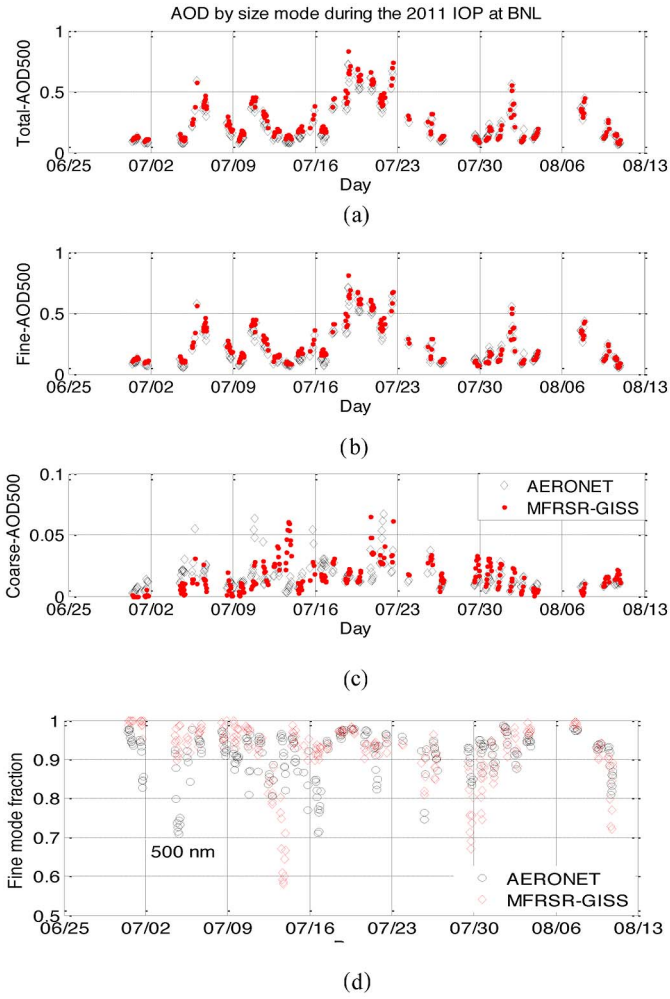

Fig. 2. Aerosol optical depth by size. (a) All size modes. (b) Fine mode. (c) Coarse mode. (d) Fine-mode fraction as measured by (in red) the MFRSR and (in black) the Cimel sunphotometer.

The AOD values retrieved were compared with the values of AOD determined from Cimel data provided by AERONET, for which the Rayleigh, NO_2, and O_3 contributions were also removed from the TOD, as with the MFRSR data.

IV. Results

A. Comparison of Optical Parameters Retrieved with MFRSR and Cimel

Within the GISS MFRSR aerosol retrieval approach [40], the underlying parameters of the assumed aerosol particle size distribution were obtained allowing for apportionment of AOD to fine- and coarse-mode aerosols through the Mie scattering theory. The Cimel approach presented earlier and described in [12]–[14] and [45] is solely based on direct spectral radiances

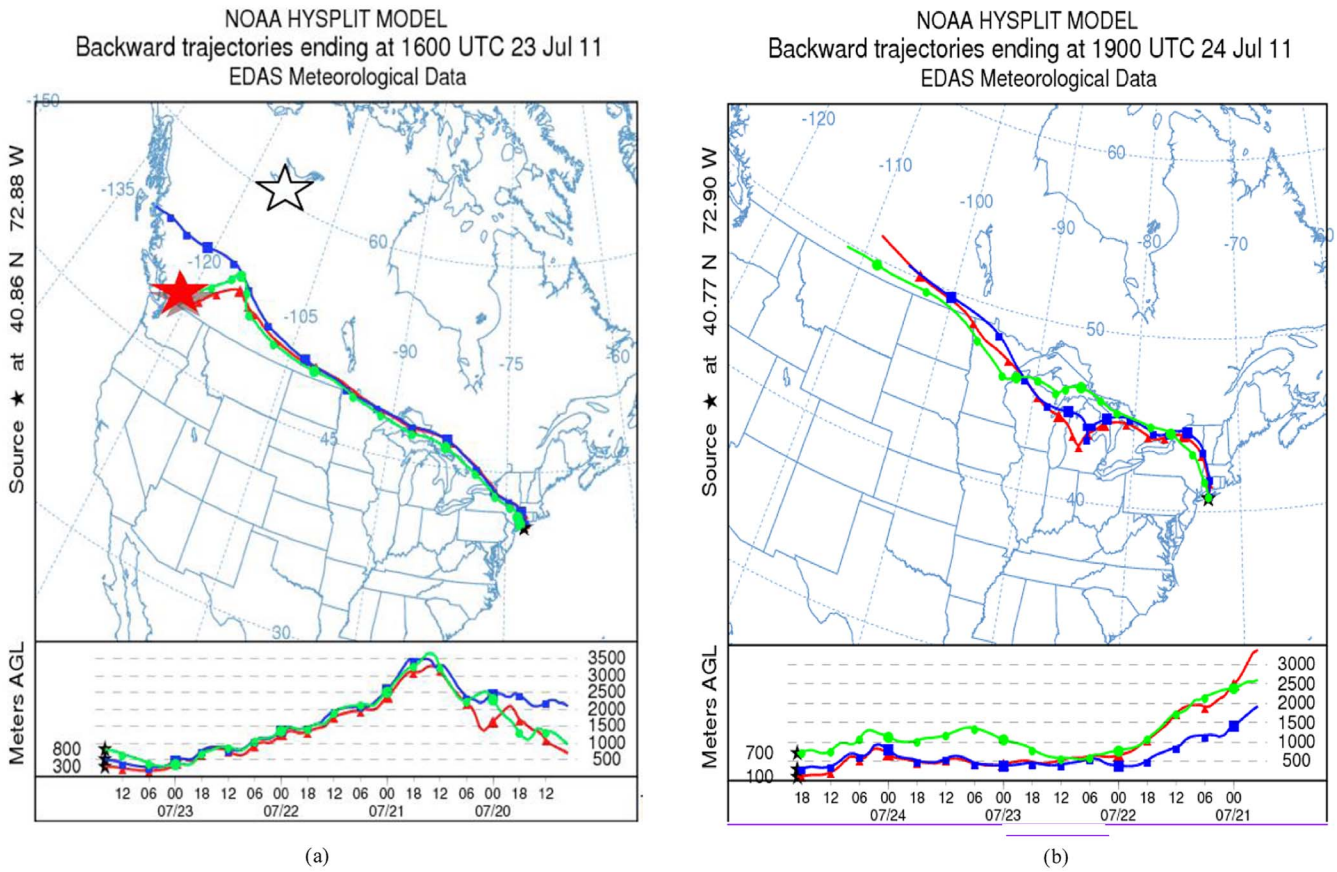

Fig. 3. HYSPLIT back three-day back trajectories [46] calculated for end time (a) 16:00 UTC July 23 and (b) 19:00 UTC July 24, 2011. The circles are shown at 6-h intervals. The red star shows the location of Kelowna in British Columbia, Canada, where the fires shown in Fig. 5(b) and (c) were observed on July 19 and 20. The white star represents the area just south of the Great Slave Lake, where the OMI and MODIS satellites observed intense fire outbreaks illustrated in Fig. 5(a) and (d) observed in the Long Island area on August 2 [47].

and the use of the algorithm providing AOD and fine/coarse-mode AOD. The time series of total AOD retrieved from MFRSR and Cimel is presented in Fig. 2 along with the fine and coarse components. Data gaps in the time series result from cloud contamination (as well as the lack of data at night).

The total AOD is consistently high during the period between July 18 and 24 and clearly dominated by the fine mode. Throughout the period, the fine mode is predominant on the days with high AOD values. The discrepancies in the fine-mode fractions on July 14 and 29 are attributed to the small values of AOD.

B. Aerosol Sources and Transport During High-AOD Periods

The sustained event during July 18–24 triggered our attention, and therefore, we looked into the possible exogenous sources of these aerosols using a combination of methods, including backward trajectories, satellite images, and chemical composition measured by an aerosol mass spectrometer.

To understand the causes of the high-AOD events, we first examined back trajectories using the HYSPLIT procedure [46]. The HYSPLIT (Hybrid Single Particle Lagrangian Integrated Trajectory) model was used to compute back trajectories for air parcels arriving at the surface at the BNL site on July 23 and 24, 2011, which are illustrated in Fig. 3.

During that period, conditions were dry enough that summer thunderstorms triggered one or two new forest fires every day as reported by the Canadian Interagency Forest Fire Service (http://www.ciffc.ca/). The smoke of fires observed in Kelowna [indicated by the red star in Fig. 3(a)] located in the proximity of Vancouver on July 19 and 20 (see Fig. 4) was detected in Long Island on July 23 and 24, respectively, and confirmed by AMS analysis illustrated in Fig. 5.

The source of the trajectory, the low altitude at which these air parcels arrived at the Long Island site, and the lack of precipitation along the trajectory path all support the conclusion that the sources of the observed fine particles are the Canadian forest fires.

The smoke event observed by the Moderate Resolution Imaging Spectroradiometer (MODIS) satellite near Great Slave Lake on July 23, 2012 and shown in Fig. 4(d) was also detected in the Long Island area on August 2, as reported in [47]. The location of the fires detected by MODIS is indicated by the white star in Fig. 3(a) found in the proximity of the Great Slave Lake.

An Ozone Monitoring Instrument (OMI) image [48] over the period from July 9 through 12, 2011, illustrates tropospheric NO_2 column concentrations over western Canada; NO_2 concentrations south of the center of Great Slave Lake appear to be the highest (in orange) in Fig. 4(a). Further investigation based on Canadian government releases indicated that from

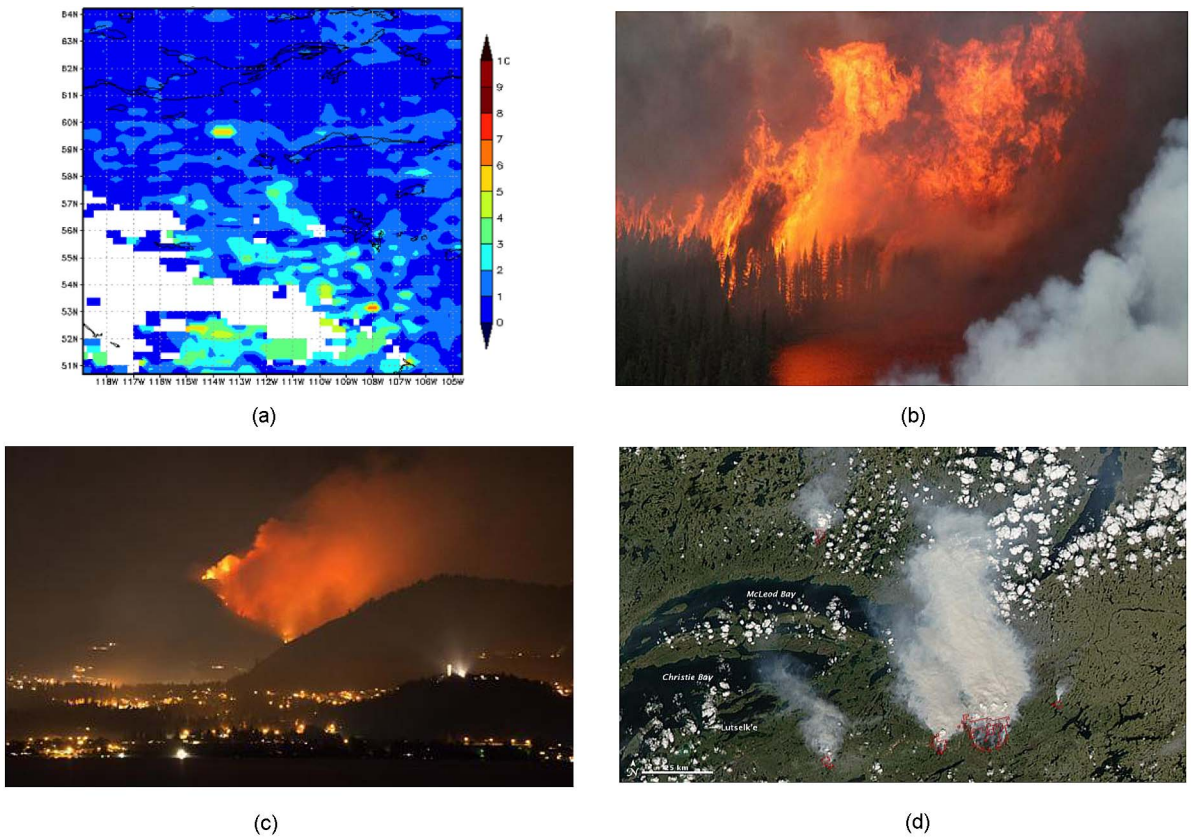

Fig. 4. (a) Smoke from fires detected by the OMI instrument on NASA's Aura satellite. This image shows NO_2 column concentrations (in units 10^{16} molecules cm^{-2}) from July 9 through 12 [8]. (b) and (c) Fires observed at Kelowna in British Columbia, Canada (just northeast of Vancouver) on July 19 and 20, 2011 [49]. (d) Fires and smoke observed on July 23, 2011 near the northeast tip of Great Slave Lake by MODIS on Aqua satellite [50]. As shown on the bottom left of this image, the scale is 25 km.

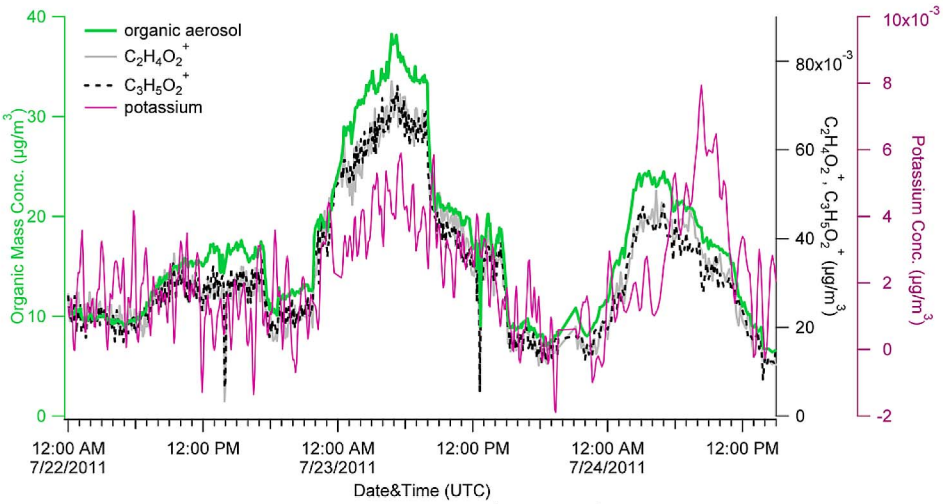

Fig. 5. Enhanced BBOA tracer ions—potassium, $C_2H_4O_2^+$, and $C_3H_5O_2^+$—observed on July 23 and 24, 2011.

July 13 to the end of the month, eight wildfires were burning in the Waterways Area, located in the northeastern part of the province (North West Territories). The NO_2 column concentrations from those fires are visible in the lower part of this image (indicated in the figure by yellow and orange) and extend from extreme northeastern Alberta into northwestern Saskatchewan.

The intensity of these fires is shown in Fig. 4(b) and (c), which shows burning on the edge of Kelowna, British Columbia, northeast of Vancouver on July 19 and 20, 2011, respectively [49], [red star in Fig. 3(a)] and, as mentioned above, were detected in Long Island on July 23 and 24, respectively, as measured by the AMS (see Fig. 5). The fires captured by NASA's MODIS instrument aboard the Aqua satellite on July 23 [50] are shown in Fig. 4(d) and are indicated by the white star in Fig. 3(a). The fires located near Great Slave Lake were also reported by the Canadian Interagency Forest Fire Service (http://www.ciffc.ca/) and have been investigated

in [47]. Again, the HYSPLIT back trajectories in Fig. 3 are consistent with the location of the fire events described above.

Attribution of the aerosol to forest fire emissions was examined using aerosol mass spectrometer measurements preformed at BNL during the IOP campaign. During this period, two high OA loading events occurred in association with elevated concentrations of three biomass burning tracer ions in the HR-ToF-AMS spectra: potassium, $C_2H_4O_2^+(m/z\ 60)$, and $C_3H_5O_2^+(m/z\ 73)$ (see Fig. 5). Particle phase potassium is a well-known tracer for biomass burning emissions in the atmosphere [51]–[53], whereas the signals of $C_2H_4O_2^+$ and $C_3H_5O_2^+$ in the AMS spectra were found to tightly correlate with levoglucosan—a major pyrolysis product of wood tissue during burning—in aerosols [54], [55].

In addition to this extended episode of biomass burning detection, a second event was examined and described in [47] on August 2 in a separate study of black carbon analysis using single particle soot photometer (SP2) and AMS. The fact that multiple events are occurring with the same characteristics supports our overall observations.

V. Conclusion

This paper has presented time series of aerosol optical depth and fine-mode fraction for the summer 2011 period simultaneously using measurements by an MFRSR and a Cimel sunphotometer. In comparing these two instruments, we found very good consistency for both AOD and fine-mode fraction, except for cases with very low AOD where the retrievals are expected to have higher errors. The good agreement illustrates that the relatively inexpensive and portable MFRSR can serve as a useful tool in diagnosing aerosol pollution events.

In analyzing the data, we found episodes of high aerosol optical depth between July 18 and 24, which were then studied in detail to determine the source of these aerosols. Source attribution was determined based on back trajectories and chemical analysis of aerosol composition using the AMS, demonstrating the strong contribution of transported plumes to the air quality at the measurement site. The attribution of the aerosol to forest fire sources confirmed by measurements with the aerosol mass spectrometer, particularly of high concentrations of biomass burning tracer ions $C_2H_4O_2^+$ and $C_3H_5O_2^+$ together with high concentrations of potassium indicates enhanced aged biomass burning aerosols. HYSPLIT backward trajectories find the sources to be Canadian fires burning in Kelowna, near Vancouver, western Canada. These hypotheses have been also confirmed by MODIS images and local news reports. These observations demonstrate that smoke from distant forest fires can be a major component of aerosol at sites quite remote from the source. Biomass smoke can be lofted into the middle and upper troposphere and can be transported over large distances in the atmosphere. Consequently, even the most remote regions of the Earth are not immune from its presence [30], [56].

Acknowledgment

D. V. Vladutescu would like to thank Dr. S. E. Schwartz for the insightful comments and suggestions made throughout this paper and the FAST Program of the U.S. DOE Office of Education. The authors would like to thank A. Sedlacek and S. Springston, Principal Investigators of the Aerosol Life Cycle IOP at BNL, for facilitating this research and Dr. M. Alexandrov for providing a software implementation of the NASA-GISS algorithm to process the MFRSR data sets.

References

[1] J. A. Ogren, "A systematic approach to *in situ* observations of aerosol properties," in *Aerosol Forcing of Climate*, R. J. Charlson and J. Heintzenberg, Eds. New York: Wiley, 1995, pp. 215–226.

[2] S. E. Schwartz, "The whitehouse effect—Shortwave radiative forcing of climate by anthropogenic aerosols: An overview," *J. Aerosol Sci.*, vol. 27, no. 3, pp. 359–382, Apr. 1996.

[3] S. Nemesure, R. Wagener, and S. E. Schwartz, "Direct shortwave forcing of climate by the anthropogenic sulfate aerosol: Sensitivity to particle size, composition, and relative humidity," *J. Geophys. Res.*, vol. 100, no. D12, pp. 26 105–26 116, 1995.

[4] A. Seaton, D. Godden, W. MacNee, and K. Donaldson, "Particulate air pollution and acute health effects," *Lancet*, vol. 345, no. 8943, pp. 176–178, Jan. 1995.

[5] B. Roy, R. Mathur, A. B. Gilliland, and S. C. Howard, "A comparison of CMAQ-based aerosol properties with IMPROVE, MODIS, and AERONET data," *J. Geophy. Res.*, vol. 112, p. D14 301, Jul. 2007.

[6] P. Doraiswamy, C. Hogrefe, W. Hao, K. Civerolo, J. Y. Ku, and G. Sistla, "A retrospective comparison of model based forecasted PM2.5 concentrations with measurements," *J. Air Waste Manage. Assoc.*, vol. 60, no. 11, pp. 1293–1308, Nov. 2010.

[7] M. D. Alexandrov, A. A. Lacis, B. E. Carlson, and B. Cairns, "Characterization of atmospheric aerosols using MFRSR measurements," *J. Geophy. Res.*, vol. 113, p. D08204, Apr. 2008.

[8] M. Bustamante, F. Moshary, B. Gross, and S. Ahmed, "Testing and development of a multi-filter rotating shadowband radiometer network for distributed monitoring of aerosol optical depth and fine mode fraction on US northeast region," in *Proc. IEEE Int. IGARSS*, 2008, pp. 1383–1386.

[9] D. V. Vladutescu, Y. Wu, B. Gross, F. Moshary, S. Ahmed, M. Razani, and R. Blake, "Remote sensing instruments used for measurement and model validation of optical parameters of atmospheric aerosols," *IEEE Trans. Instrum. Meas.*, vol. 61, no. 6, pp. 1733–1746, Jun. 2012.

[10] L. Harrison, J. Michalsky, and J. Berndt, "Automated multi-filter rotating shadowband radiometer: An instrument for optical depth and radiation measurements," *Appl. Opt.*, vol. 33, no. 22, pp. 5118–5125, Aug. 1994.

[11] G. Box, G. Taha, and M. Kuzmanoski, "Long-term atmospheric monitoring in Sydney using an MFRSR," in *Proc. IGARSS*, 2001, vol. 1, pp. 81–83.

[12] O. Dubovik and M. D. King, "A flexible inversion algorithm for retrieval of aerosol optical properties from sun and sky radiance measurements," *J. Geophys. Res.*, vol. 105, no. D16, pp. 20 673–20 696, Aug. 2000.

[13] O. Dubovik, T. Yokota, and Y. Sasano, "Improved technique for data inversion and its application to the retrieval algorithm for ADEOS/ILAS," *Adv. Space Res.*, vol. 21, no. 3, pp. 397–403, 1998.

[14] B. N. Holben, T. F. Eck, I. Slutsker, D. Tanre, J. P. Buis, A. Setzer, E. Vermote, J. A. Reagan, Y. Kaufman, T. Nakajima, F. Lavenu, I. Jankowiak, and A. Smirnov, "AERONET—A federated instrument network and data archive for aerosol characterization," *Remote Sens. Environ.*, vol. 66, pp. 1–16, Jan. 1998.

[15] "Multifilter rotating shadowband radiometer, multifilter radiometer and normal incidence radiometer ARM," U.S. Dept. Energy, Washington, DC, DOE/SC-AM/TR-059, Feb. 2011.

[16] M. D. Alexandrov, P. Kiedron, J. J. Michalsky, G. Hodges, C. J. Flynn, and A. A. Lacis, "Optical depth measurements by shadow-band and their uncertainties," *Appl. Opt.*, vol. 46, no. 33, pp. 8027–8038, Nov. 2007.

[17] *Concentrating Solar Power. Best Practices Handbook for the Collection and Use of Solar Resource Data*, Nat. Renew. Energy Lab., Golden, CO, NREL/TP-550-47465, Sep. 2010. [Online]. Available: http://www.nrel.gov/docs/fy10osti/47465.pdf

[18] H. A. Gannet, D. H. Lowenthal, G. Chirokova, R. D. Boyrs, and C. Wiedinmyer, "Persistent daily new particle formation at a mountain-top location," *J. Atmos. Environ.*, vol. 45, no. 24, pp. 4111–4115, Aug. 2011.

[19] W. Gao, D. Schmoldt, and J. R. Slusser, *UV Radiation in Global Climate Change: Measurements, Modeling and Effects on Ecosystems*. Berlin, Germany: Springer-Verlag, 2009.

[20] R. M. Mitchell and B. W. Forgan, "Aerosol measurement in the Australian outback: Intercomparison of sun photometers," *J. Atmos. Ocean. Technol.*, vol. 20, no. 1, pp. 54–66, Jan. 2003.

[21] J. Michalsky, F. Denn, C. Flyn, G. Hodges, P. Kiedron, A. Koontz, J. Schlemer, and S. E. Schwartz, "Climatology of aerosol optical depth in north-central Oklahoma:1992–2008," *J. Geophys. Res.*, vol. 115, p. D07203, Apr. 2010.
[22] G. Hodges, "Multifilter rotating shadowband radiometers mentor report and baseline surface radiation network submission status," in *Proc. 15th ARM Sci. Team Meeting*, Mar. 2005, pp. 1–15.
[23] *CIMEL Sunphotometer (CSPHOT)*, ARM, Climate Res. Facility, U.S. Dept. Energy, Washington, DC, ARM, DOE/ SC-ARM/TR-056, Jan. 2011. [Online]. Available: http://www.arm.gov/publications/tech_reports/handbooks/csphot_handbook.pdf
[24] J. T. Jayne, D. C. Leard, X. Zhang, P. Davidovits, K. A. Smith, C. E. Kolb, and D. R. Worsnop, "Development of an aerosol mass spectrometer for size and composition analysis of submicron particles," *Aerosol Sci. Technol.*, vol. 33, no. 1/2, pp. 49–70, Jul. 2000.
[25] J. L. Jimenez, J. T. Jayne, Q. Shi, C. E. Kolb, D. R. Worsnop, I. Yourshaw, J. H. Seinfeld, R. C. Flagan, X. Zhang, K. A. Smith, and J. W. Morris, "Ambient aerosol sampling with an aerosol mass spectrometer," *J. Geophys. Res.*, vol. 108, no. D7, p. 8425, 2003.
[26] M. Canagaratna, J. Jayne, J. L. Jimenez, J. A. Allan, R. Alfarra, Q. Zhang, T. Onasch, F. Drewnick, H. Coe, A. Middlebrook, A. Delia, L. Williams, A. Trimborn, M. Northway, P. DeCarlo, C. Kolb, P Davidovits, and D. Worsnop, "Chemical and microphysical characterization of ambient aerosols with the aerodyne aerosol mass spectrometer," *Mass Spectrom. Rev.*, vol. 26, no. 2, pp. 185–222, 2007.
[27] Q. Zhang, J. L. Jimenez, M. Canagaratna, N. L. Ng, I. Ulbrich, D. Worsnop, and Y. L. Sun, "Understanding organic aerosols via factor analysis of aerosol mass spectrometry: A review," *Anal. Bioanal. Chem.*, vol. 401, no. 10, pp. 3045–3067, Dec. 2011.
[28] Q. Zhang, J. L. Jimenez, D. R. Worsnop, and M. Canagaratna, "A case study of urban particle acidity and its influence on secondary organic aerosol," *Environ. Sci. Technol.*, vol. 41, no. 9, pp. 3213–3219, May 2007.
[29] J. H. Seinfeld and S. N. Pandis, *Atmospheric Chemistry and Physics: From Air Pollution to Climate Change*. Berlin, Germany: Wiley, 2006, ch. 7.
[30] G. Shaw, "Genesis of sun photometry," *J. Appl. Remote Sens.*, vol. 1, no. 1, pp. 012503-1–012503-13, Feb. 2007.
[31] J. M. Wallace and P. V. Hobbs, *Atmospheric Science*. New York: Academic, 2006, pp. 158–167.
[32] G. Myhre, "Intercomparison of satellite retrieved aerosol optical depth over the ocean," *J. Atmos. Sci*, vol. 61, no. 5, pp. 499–513, Mar. 2004.
[33] E. I. Kassianov, C. J. Flynn, T. P. Ackerman, and J. C. Barnard, "Aerosol single-scattering albedo and asymmetry parameter from MFRSR observations during the ARM Aerosol IOP 2003," *Atmos. Chem. Phys.*, vol. 7, no. 12, pp. 3341–3351, 2007.
[34] X. Qiuyun, X. Zheng, Z. Li, W. Zhang, X. Wang, J. Li, and X. Li, "Absolute spectral radiance responsivity calibration of sun photometers," *Rev. Sci. Instrum.*, vol. 81, no. 3, p. 033103, Mar. 2010.
[35] G. E. Shaw, "Error analysis of multi-wavelength sun photometry," in *Pure Applied Geophysics*. Berlin, Germany: Birkhäuser-Verlag, 1976.
[36] NASA, Goddard Space Center, AERONET, *Data-Access and Dissemination Tools*. [Online]. Available: http://aeronet.gsfc.nasa.gov/new_web/data.html
[37] P. F. DeCarlo, J. R. Kimmel, A. Trimborn, J. Jayne, A. C. Aiken, M. Gonin, K. Fuhrer, T. Horvath, D. R. Worsnop, and J. L. Jimenez, "A field-deployable high-resolution, time-of-flight aerosol mass spectrometer," *Anal. Chem.*, vol. 78, no. 24, pp. 8281–8289, 2006.
[38] A. C. Aiken, P. F. DeCarlo, J. H. Kroll, D. R. Worsnop, J. A. Huffman, K. Docherty, I. M. Ulbrich, C. Mohr, J. R. Kimmel, D. Sueper, Y. Sun, Q. Zhang, A. Trimborn, M. Northway, P. J. Ziemann, M. R. Canagaratna, T. B. Onasch, M. R. Alfarra, A. S. H. Prevot, J. Dommen, J. Duplissy, A. Metzger, U. Baltensperger, and J. L. Jimenez, "O/C and OM/OC ratios of primary, secondary, and ambient organic aerosols with a high resolution time-of-flight aerosol mass spectrometer," *Environ. Sci. Technol.*, vol. 42, no. 12, pp. 4478–4485, Jun. 2008.
[39] M. D. Alexandrov, A. Marshak, B. Cairns, A. A. Lacis, and B. E. Carlson, "Automated cloud screening algorithm for MFRSR data," *Geophys. Res. Let.*, vol. 310, no. 4, p. L04 118, 2004.
[40] M. D. Alexandrov, A. L. Lacis, B. E. Carlson, and B. Cairns, "Remote sensing of atmospheric aerosols and trace gases by means of multifilter rotating shadowband radiometer. Part 1: Retrieval algorithm," *J. Atmos. Sci.*, vol. 59, no. 3, pp. 524–543, Feb. 2002.
[41] J. E. Hansen and L. D. Travis, "Light scattering in planetary atmospheres," *Space Sci. Rev.*, vol. 16, no. 4, pp. 527–610, Oct. 1974.
[42] G. Taha and G. P. Box, "New method for inferring total ozone and aerosol optical thickness from multispectral extinction measurements using eigenvalue analysis," *Geophys. Res. Lett.*, vol. 26, no. 20, pp. 3085–3088, 1999.
[43] J. J. Michalsky, "Multilayer measurements of aerosol optical depth in the atmospheric radiation measurement and quantitative links program," *J. Geophys. Res.*, vol. 106, no. D11, pp. 12 099–12 107, 2001.
[44] M. D. Alexandrov, A. A. Lacis, B. E. Carlson, and B. Cairns, "Separation of fine and coarse aerosol modes in MFRSR data sets," *J. Geophys. Res.*, vol. 110, no. D13, p. D13204, Jul. 2005.
[45] N. T. ONeill, T. F. Eck, A. Smirnov, B. N. Holben, and S. Thulasiram, "Spectral discrimination of coarse and fine mode optical depth," *J.Geophy. Res.*, vol. 108, no. D17, p. 4559, Sep. 2003.
[46] [Online]. Available: http://ready.arl.noaa.gov/HYSPLIT.php
[47] A. J. Sedlacek, III, E. R. Lewis, L. Kleinman, J. Xu, and Q. Zhang, "Determination of and evidence for non-core-shell structure of particles containing black carbon using Single-Particle Soot Photometer (SP2)," *Geophys. Res. Lett.*, vol. 39, p. L06802, Mar. 2012.
[48] [Online]. Available: http://www.nasa.gov/mission_pages/fires/main/Canada-fire-20110715.html
[49] [Online]. Available: http://www.reuters.com/article/2009/07/20/us-fire-idUSTRE56I0LS20090720
[50] [Online]. Available: http://www.nasa.gov/mission_pages/fires/main/world/20110723-canada.html
[51] P. K. Hudson, D. M. Murphy, D. J. Cziczo, D. S. Thomson, J. A. de Gouw, C. Warneke, J. Holloway, J. R. Jost, and G. Hubler, "Biomass-burning particle measurements: Characteristic composition and chemical processing," *J. Geophys. Res.*, vol. 109, no. D23, p. D23S27, Jul. 2004.
[52] T. Reiner, D. Sprung, C. Jost, R. Gabriel, O. L. Mayol-Bracero, M. O. Andreae, T. L. Campos, and R. E. Shetter, "Chemical characterization of pollution layers over the tropical Indian Ocean: Signatures of emissions from biomass and fossil fuel burning," *J. Geophys. Res.*, vol. 106, no. D22, pp. 28 497–28 510, Nov. 2001.
[53] A. C. Aiken, B. D. Foy, C. Wiedinmyer, P. F. DeCarlo, I. M. Ulbrich, M. N. Wehrli, S. Szidat, A. S. H. Prevot, J. Noda, L. Wacker, R. Volkamer, E. Fortner, J. Wang, A. Laskin, V. Shutthanandan, J. Zheng, R. Zhang, G. Paredes-Miranda, W. P. Arnott, L. T. Molina, G. Sosa, X. Querol, and J. L. Jimenez, "Mexico City aerosol analysis during MILAGRO using high resolution aerosol mass spectrometry at the urban supersite (T0)—Part 2: Analysis of the biomass burning contribution and the non-fossil carbon fraction," *Atmos. Chem. Phys.*, vol. 10, no. 12, pp. 5315–5341, 2010.
[54] C. Mohr, J. A. Huffman, M. J. Cubison, A. C. Aiken, K. S. Docherty, J. R. Kimmel, I. M. Ulbrich, M. Hannigan, and J. L. Jimenez, "Characterization of primary organic aerosol emissions from meat cooking, trash burning, and motor vehicles with high-resolution aerosol mass spectrometry and comparison with ambient and chamber observations," *Environ. Sci. Technol.*, vol. 43, no. 7, pp. 2443–2449, Apr. 2009.
[55] Y. Sun, Q. Zhang, M. Zheng, X. Ding, E. S. Edgerton, and X. Wang, "Characterization and source apportionment of water-soluble organic matter in atmospheric fine particles (PM2.5) with high-resolution aerosol mass spectrometry and GC-MS," *Environ. Sci. Technol.*, vol. 45, no. 11, pp. 4854–4861, Jun. 2011.
[56] J. M. Wallace and P. V. Hobbs, *Atmospheric Science*. New York: Academic, 2006, pp. 158–167.

Daniela Viviana Vladutescu received the B.S.E.E. degree from Polytechnic University of Bucharest, Bucharest, Romania; the M.S. degree in electrical engineering from the New York City College of Technology, City University of New York (CUNY), Brooklyn; and the Ph.D. degree in electrical engineering from the Graduate Center, CUNY in 2008.

She is currently an Assistant Professor with the Electrical and Telecommunications Engineering Technology Department, New York City College of Technology, CUNY. Her research focus is on optics and remote sensing of the atmosphere, collaborating with several centers in remote sensing such as NOAA Cooperative Remote Sensing Science and Technology Center, Earth Science Department at Brookhaven National Laboratory, NASA Goddard Institute of Space Studies and NASA Goddard Space Flight Center, Optics Branch 5510. Her research is concentrated in the optical remote sensing of properties and concentration of atmospheric trace constituents as well as model development and model validation using land- and spaced-based remote sensing systems. Additionally, she is specialized in modern optical metrology systems used in noncontact measurements of space instruments.

Dr. Vladutescu is currently funded through National Science Foundation and NASA grants and has been the recipient of several other CUNY institutional grants (Graduate Research & Technology Initiative, Professional Staff Congress). She is a Coeditor of the EARSeL eProceedings and a member of the International Society for Optics and Photonics.

Bomidi Lakshmi Madhavan received the Ph.D. degree in physics from Andhra University, Visakhapatnam, India, in 2009. His doctoral research focused on a combination of aerosol *in situ* and remote sensing measurements including radiometer and micropulse lidar together with radiative transfer simulations to measure heat flux gradients.

Since 2009, he has been a Postdoctoral Research Fellow with NOAA CREST, where he has been involved in the data processing of multifilter rotating shadowband radiometer, microwave radiometer, and Raman lidar observation measurements to simultaneously extract cloud optical depth and effective radius. Since October 2011, he has been a Postdoctoral Fellow with the Department of Chemical Engineering, Indian Institute of Technology, Bombay, India, in an Indo-French project aimed at developing a methodology for quantifying particulate mass using lidar signals. His research interests include atmospheric aerosols, radiative transfer modeling, remote sensing techniques, aerosol–cloud interaction studies, development of aerosol retrieval algorithms, and multivariate factor analytic techniques (e.g., principal component analysis and positive matrix factorization).

Barry M. Gross received the B.A. degree in physics from Yeshiva University, New York, in 1987 and the Ph.D. degree in electrical engineering from the City College of New York, New York, in 1992.

He is currently a Professor with the Department of Electrical Engineering, City College of New York, where he is working on a variety of projects. This includes the analysis of multispectral re?ectance data from both geostationary and polar-orbiting satellites for the analysis of aerosols in urban coastal areas and the use of combined active and passive sensors for the improved detection and quantification of trace gases and aerosols and the improved retrieval of ocean color properties in coastal areas through improved atmospheric correction procedures. He is currently funded through the NOAA-CREST center and New York State Energy Research and Development Authority and is a Research Associate with the National Science Foundation-Mid Infrared Technologies for Health and the Environment center. He has authored or coauthored more than 40 journal articles.

Dr. Gross is a member of The International Society for Optical Engineers.

Qi Zhang received the Ph.D. degree in atmospheric chemistry from the University of California, Davis, in 2002.

She is an Associate Professor with the Department of Environmental Toxicology, University of California, Davis. Her research interests include aerosol mass spectrometry, field and laboratory studies of atmospheric aerosols, and integrated analysis of global aerosol mass spectrometry data sets.

Shan Zhou received the B.S. degree in atmospheric science from SunYat-sen University, Guangzhou, China, in 2011. She is currently working toward the Ph.D. degree in the Atmosphere Science Graduate Group, University of California, Davis, conducting research in Prof. Q. Zhang's group.

Her research interest includes in-depth analysis of atmospheric field measurement data acquired with aerosol mass spectrometers in order to better understand the sources, processes, and chemical and physical properties of organic and inorganic particles.